The Orbital Angular Momentum Fiber Modes for Magnetic Field Sensing

Fufei Pang, Haoqiang Zheng, Huanhuan Liu, Junfeng Yang, Na Chen, Yana Shang, Siddharth Ramachandran, and Tingyun Wang

***Abstract*— We have proposed a magnetic field sensor using orbital angular momentum (OAM) $L = \pm 1$ modes, corresponding to right- and left- handed circular polarization, respectively, in a vortex fiber that supports propagation of these modes. These two circularly polarized OAM modes produce a phase difference under the Faraday effect, which results in the rotation of optical petal when both OAM modes pass through a polarizer. A photodetector is used to detect the intensity variation of the output from the polarizer followed by a slit. By using this method, we have experimentally achieved the superposition of OAM modes with the vector representation of HE_{21} mode for magnetic field sensing. And a magnetic field sensitivity of $3.31\%/T$ can be reached at the width ratio of the slit to the petal-like pattern of 0.35 ± 0.02. The obtained experimental results prove the successful implementation of this proof-of-concept principle, showing its potential applications in all-fiber current sensing.**

***Index Terms*— Fiber optics sensors, Faraday effect, magnetic field, vortex fiber.**

I. Introduction

THE orbital angular momentum (OAM) beams have attracted much attention in many fields recently including telecommunications [1]–[4], atom trapping [5], tweezers [6], quantum information science [7], [8], *etc*. Different from the conventional Gaussian beam, the OAM beam has a unique feature of helical phase front. Such helical phase front of OAM beams associated with the spin angular momentum (SAM), known as left- (L-) or right-handed (R-) circular polarization, can be explored for interacting with matter and thus investigating the new physical phenomena [9]–[13].

The Faraday-rotation-effect based magnetic field measurement is one of the most typical and important applications. Combining the OAM and the SAM, Shi *et al.* have studied the rotation of OAM beams propagating in free space through an Rb atomic vapor chamber under magnetic field variations [12]. The hypersuperposition of the OAM and the SAM was achieved through a Sagnac interferometer. But the experiment had to be carried out in a high temperature atomic vapor (89°C), which greatly limits the potential applications. Alternatively, to solve the issues related to the magnetic-field-sensitive medium, our group have successfully demonstrated the use of the compositing two OAM beams in a Sagnac configuration comprising a $Bi_4Ge_3O_{12}$ (BGO) magneto-optic crystal to realize the magnetic field sensing [13]. Nevertheless, the OAM beams for sensing are produced in free space and require complex bulk optical components, which are susceptible to environmental disturbances and difficult to achieve alignment and are not suitable for practical applications.

In parallel, special optical fibers have been developed to propagate OAM modes, which are achieved either by step-index designs [3], air-cores [14], inverse parabolic index profiles [15] or photonic crystal designs [16]. Such OAM fibers featuring an annular core have the intrinsic advantages of fibers for magnetic field sensing including a high degree of insulation, their lightweight nature, small footprint, fast response, and potentially low costs [17]. The magnetic field sensing can be realized by detecting the phase change between the two orthogonal modes with circularly polarization (R- and L-) [18]. In order to achieve magnetic field sensing in OAM fibers, the key is to determine and assign two orthogonal modes to detect the Faraday-effect-induced phase difference. However, the study of OAM fibers for magnetic field sensing has not been reported yet.

In this letter, we have proposed and demonstrated a vortex fiber with the superposition of OAM modes for magnetic field sensing for the first time to the best of our knowledge. The used vortex fiber with large refractive index difference has been demonstrated as a new physical channel supporting ± 1 OAM modes for 1.1 km-long optical fiber communication [3]. Attributed to such large refractive index difference, the vortex fiber lifts the near degeneracy between the desired $OAM_{\pm}$ and parasitic TM_{01} and TE_{01}, hence minimizing modal crosstalk between them. Since OAM modes transforming from the superposition of vector modes of HE_{21} possess the R- and L- circularly polarizations, the phase difference produced under the Faraday effect can be determined analog to the free space OAM beams by exploring two orthogonal circularly polarized OAM modes in vortex fiber. In order to simplify the detection scheme and its installation in real applications, instead of an image acquisition system, for example CCD camera, a photodetector is used to recognize the intensity variation from the polarizer followed by a slit. By this method, we have achieved experimentally the superposition of OAM

Manuscript received February 21, 2019; revised April 3, 2019; accepted April 14, 2019. Date of publication April 18, 2019; date of current version May 15, 2019. This work was supported in part by the Natural Science Foundation of China under Grant 61635006, Grant 61605108, Grant 61875118, and Grant 61675125, in part by the Shuguang Program under Grant 16SG35, and in part by the U.S. National Science Foundation under Grant ECCS-1610190. *(Corresponding author: Fufei Pang.)*

F. Pang, H. Zheng, H. Liu, J. Yang, N. Chen, Y. Shang, and T. Wang are with the Key Laboratory of Specialty Fiber Optics and Optical Access Networks, Shanghai University, Shanghai 200444, China, and also with the Joint International Research Laboratory of Specialty Fiber Optics and Advanced Communication, Shanghai Institute for Advanced Communication and Data Science, Shanghai University, Shanghai 200444, China (e-mail: ffpang@shu.edu.cn).

S. Ramachandran is with the Department of Electrical and Computer Engineering, Boston University, Boston, MA 02215 USA (e-mail: sidr@bu.edu).

Color versions of one or more of the figures in this letter are available online at http://ieeexplore.ieee.org.

Digital Object Identifier 10.1109/LPT.2019.2911976

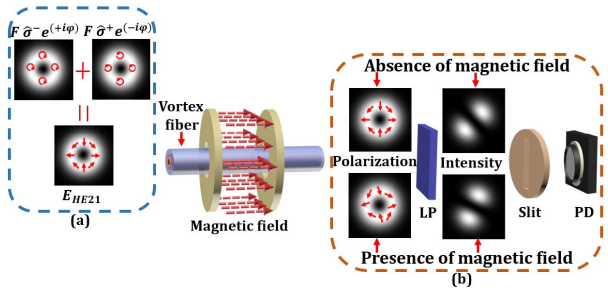

Fig. 1. Schematic diagram of the vortex fiber for magnetic field sensing. Distribution of intensity and the polarization of the superposition of OAM modes and the generated petal pattern when it passes through a linear polarizer (LP). Under the magnetic field, the petal pattern rotates, the light intensity passing through the slit then changes.

modes in the vortex fiber for magnetic field sensing with sensitivity of approximate 3.31%/T. The obtained experimental results prove the successful implementation of this proof-of-concept principle.

II. Sensing Principle

Figure 1 illustrates the principle of magnetic field sensing based on the superposition of OAM modes in vortex fiber. The OAM modes are superposition of HE_{21} modes as $OAM^{\mp}_{\pm 1} = HE^{even}_{21} \pm iHE^{odd}_{21}$, which present circular polarizations. To qualify the OAM modes as the media of the Faraday magnetic-optic effect, these two $OAM^{\mp}_{\pm 1}$ modes can be denoted as $e_{\pm 1,0} = F_{\pm 1,0}(r,z)\hat{\sigma}^{\mp}\exp(\pm i\varphi)$ in the circular polarization coordinate system, where $F_{\pm 1,0}(r,z)$ is the field amplitude at propagation distance z, φ is the azimuthal angle and $\hat{\sigma}^{\mp}$ represent R- and L- handed circular polarization, respectively. The magnetic field sensor principle can be analyzed by using Jones matrix. For computational simplicity in the discussion below we consider a vortex with the initial field amplitude [19], [20]:

$$F = F_{+1,0}(r, z=0) = F_{-1,0}(r, z=0) = E_0(r/w)\exp(-r^2/w^2) \tag{1}$$

where E_0 and w are the characteristic amplitude and beam size in the plane z = 0.

The superposition of OAM^{-}_{+1} and OAM^{+}_{-1} modes can be expressed in the Jones' vector as:

$$\begin{aligned} E_{superposition} &= \frac{\sqrt{2}}{2}\exp(+i\varphi)\begin{bmatrix}0\\1\end{bmatrix} F_{+1,0}(r, z=0) \\ &\quad + \frac{\sqrt{2}}{2}\exp(-i\varphi)\begin{bmatrix}1\\0\end{bmatrix} F_{-1,0}(r, z=0) \\ &= \frac{\sqrt{2}\,F}{2}\begin{bmatrix}\exp(-i\varphi)\\ \exp(+i\varphi)\end{bmatrix} \end{aligned} \tag{2}$$

Figure 1(a) plots the intensity of the two OAM modes, presenting donut profile and opposite circular polarization directions. According to the relationship in Eq. (2), the superposition of OAM modes can be represented as HE_{21} mode. After both OAM modes transmit through the vortex fiber, its polarization distribution change can be detected by using a polarizer followed by a near infrared camera [13]. Here, in order to simply the detection scheme, we replace the image acquisition system by a slit followed by a photodetector (PD). The rotation of the petal pattern induced by polarization change can be conveniently converted to the change of optical power.

When a magnetic field is applied parallel to the axis of the vortex fiber, it induces a magneto-optical circular birefringence given by $\Delta\varphi = 2\pi(n_{\hat{\sigma}-} - n_{\hat{\sigma}+})d/\lambda$. Here, $n_{\hat{\sigma}-}$ and $n_{\hat{\sigma}+}$ are the refractive indices of the R- and L- circularly polarized modes of the vortex fiber, respectively, where λ is the optical wavelength and d is the length of vortex fiber subjected to magnetic field. The phase difference $\Delta\varphi$ that is induced by the Faraday effect can be regarded as being equivalent to a polarization rotation, which is described by the Verdet law $\Delta\varphi/2 = VBd$, where the Verdet constant V provides a quantitative measure of the Faraday effect and B is the magnetic field intensity. The polarization of the superposition of OAM beams rotates depending on the Faraday effect, as illustrated in Fig. 1 (b). Hence, although there is no change in the donut-shaped intensity profile, the petal pattern after the polarizer rotates an angle ($\theta = VBd$) determined by the applied magnetic field.

The circular birefringence induced by the Faraday effect can be represented by the Jones matrix $J_B = \begin{bmatrix}\exp(+iVBd) & 0\\ 0 & \exp(-iVBd)\end{bmatrix}$ in circular polarization coordinates. The whole transmission process can be expressed in the Cartesian coordinates as

$$\begin{aligned} E_{out} &= J_P \cdot A \cdot J_B \cdot E_{superposition} \\ &= \begin{bmatrix}1 & 0\\ 0 & 0\end{bmatrix}\frac{1}{\sqrt{2}}\begin{bmatrix}1 & 1\\ -i & i\end{bmatrix}\begin{bmatrix}\exp(+iVBd) & 0\\ 0 & exp(-iVBd)\end{bmatrix} \\ &\quad \times \frac{\sqrt{2}\,F}{2}\begin{bmatrix}\exp(-i\varphi)\\ \exp(+i\varphi)\end{bmatrix} \\ &= F\cdot\begin{bmatrix}\cos(\varphi - VBd)\\ 0\end{bmatrix} \end{aligned} \tag{3}$$

where $A = \frac{1}{\sqrt{2}}\begin{bmatrix}1 & 1\\ -i & i\end{bmatrix}$ refers to the matrix for transformation of circular coordinates into Cartesian coordinates, $J_P = \begin{bmatrix}1 & 0\\ 0 & 0\end{bmatrix}$ is the Jones matrix of the polarizer.

Without loss of generality, we assume that E_0 is normalized. Therefore, the intensity distribution of the superposition of OAM beams yields

$$\begin{aligned} I(r,\varphi) &= |E_{out}(r,\varphi)|^2 \\ &= \frac{1}{2}\left(\frac{r}{w}\right)^2\cdot\exp\left(-\frac{2r^2}{w^2}\right)\cdot\{1+\cos[2(\varphi - VBd)]\} \end{aligned} \tag{4}$$

Equation (4) shows that the petal-like pattern has a distribution with circular symmetry with the $\cos[2(\varphi - VBd)]$ function in the azimuthal angle. If a slit is introduced after the polarizer, it only allows the azimuthal angle that is parallel to the slit axis to be filtered out. Light intensity after passing through a slit can be written as:

$$I_{total} = \int_{-\infty}^{+\infty}\int_{-\infty}^{+\infty} I(x,y)\cdot h(x)\,dxdy \tag{5}$$

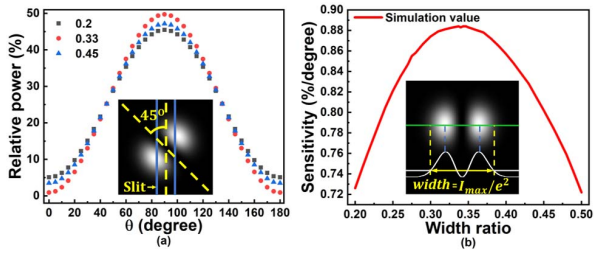

Fig. 2. (a) Under different width ratio of slit to petal-like patterns, the light intensity changes with the Faraday rotation angle. (b) The relationship between the width ratio and the sensitivity at this working point.

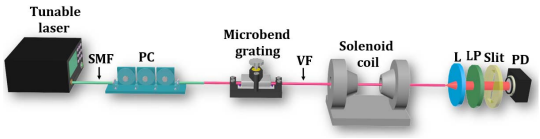

Fig. 3. The experimental setup of measuring magnetic field. SMF: single-mode fiber; PC: polarization controller; VF: vortex fiber; L: Lens; LP: linear polarizer; PD: optical photodetector.

where $I(x, y)$ is an expression of $I(r, \varphi)$ in Cartesian coordinate, $h(x) = \begin{cases} 1 & |x| < a/2 \\ 0 & |x| > a/2 \end{cases}$ is the transfer function of the slit, a is the slit width.

As the petal-like pattern rotates along the azimuthal direction due to the Faraday effect under magnetic field variation, the light intensity from the slit will change. Figure 2(a) simulates the variation of light intensity with Faraday rotation angle θ after the slit according to Eq. (5). In order to obtain a linear response, the working point should be near 45 degrees corresponding to the direction of the yellow dashed line between the two petals labeled in the inset of Fig. 2(a). Since the slit is used, the sensitivity also depends on the width of the slit and the diameter of the output pattern. In order to characterizing their impact, we define the width ratio as the ratio of slit width to petal pattern diameter (the diameter refers to the position $1/e^2$ intensity). Figure 2(b) shows that as the ratio increases, the change trend of sensitivity approximates a parabola, and the maximum value 0.88%/degree is obtained at 0.35 ± 0.02 near this working point.

III. Experimental Results and Discussions

The experimental setup of applying the vortex fiber for magnetic field sensing is shown in Fig. 3. The detailed refractive index profile of the vortex fiber and its end-face are given in Fig. 4(a). The vortex fiber has coaxial rod and tube waveguide structures with high refractive index difference. According to Eq. (2), the superposition of OAM modes is equivalent to HE_{21}. By applying a mechanical long period grating (LPG) on the vortex fiber, the fundamental mode of the vortex fiber can be easily coupled to the HE_{21} mode. Here we design a UV-resin periodic embossment grating and fabricate it by using a 3D printer. Then, the vortex fiber passes through a solenoid coil which induces magnetic field parallel to the direction of light propagation to generate the Faraday effect in the sensing fiber. Finally, the output of the vortex fiber

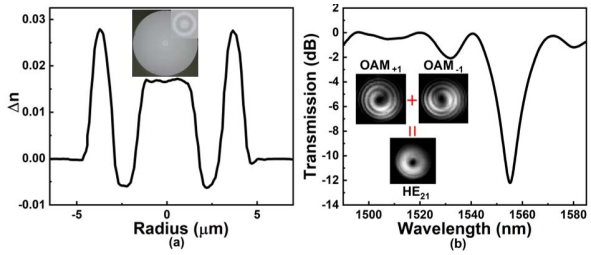

Fig. 4. (a) Refractive index profile and end view of the vortex fiber. (b) LPG resonant spectrum used to deduce HE_{21} mode conversion level.

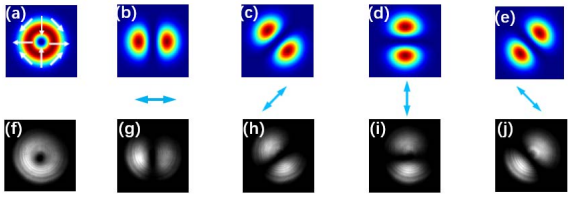

Fig. 5. Theoretical (a) and experimental (f) images taken by the InGaAs camera in absence of polarizer, and theoretical (b-e) and experimental (g-j) petal-like patterns in presence of polarizer at 0°, 45°, 90°, 135° polarization orientations.

is collimated and passes through the polarizer, slit and PD successively.

The vortex fiber is pressed by the embossment grating to form a microbend LPG which can excite the HE_{21} at the phase matching wavelength $\lambda_{\text{res}} = (n_{HE_{11}} - n_{HE_{21}})\ \Lambda$. The polarization direction of the excited HE_{21} mode can be adjusted by using the polarization controller (PC) on the input SMF. Figure 4(b) shows the transmission spectrum. When the grating period Λ is 520 μm, the measured conversion efficiency exceeds 94% at the resonance wavelengths $\lambda_{res} = 1555.2$ nm. In order to confirm the superposition of the opposite circularly polarized state, the output of the vortex fiber is split by a quarter wave plate followed a PBS. In the inset of Fig. 4(b), the split outputs present an equal intensity and an opposite vortex charge.

Moreover, to confirm the mode of HE_{21} mode rather than TE_{01} and TM_{01} modes after the vortex fiber, the output pattern is observed as shown in Fig. 5(f). A twin-petal pattern is experimentally observed after the polarizer, as shown in Figs.5(g)-5(j). By rotating the analyzer direction (indicated by the inset arrow in Fig. 5), the output petal pattern direction rotates correspondingly, which is consistent with the simulation as shown in Figs. 5(b)-5(e). Therefore, the excited mode refers to the HE_{21} mode.

The magnetic field sensing is further investigated by using the superposition of $OAM_{\pm 1}^{\mp}$ modes in the form of HE_{21} in the vortex fiber. In order to obtain the linear response, the polarizer is adjusted so that the direction of the petal-like pattern is at an angle of 45 degrees to the slit. In the measurement, petal-like pattern width at the slit was 3.42 mm. The application of different magnetic field intensities (0 to 0.406 Tesla) to the vortex fiber with effective length of 12 cm will cause the petal-like patterns to rotate based on the Faraday effect, the light intensity after the slit then changes (indicated by Eq. (5)).

The change in light intensity after slit was measured by the optical power meter with the varying magnetic field intensities.

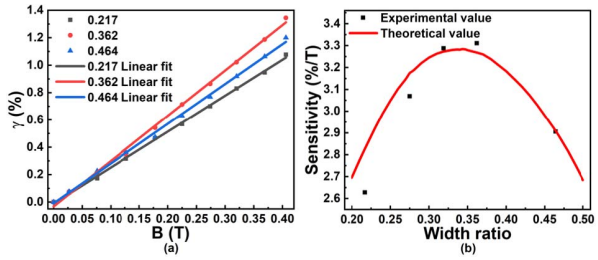

Fig. 6. (a) Variation of γ with respect to the magnetic field when the width ratios of slit to petal-like patterns are 0.217, 0.362, 0.464; (b) the theoretical and experimental sensitivities in the relationship of width ratio.

In order to obtain the sensitivity that is independent of the optical power, we include a parameter (γ):

$$\gamma = \frac{\Delta I_{total}}{I} \tag{6}$$

where ΔI_{total} is the power change after the slit with increasing magnetic field strength; I is the input power of the slit that equals to 0.729 mW when the output power of the light source is 6.5 mW.

Figure 6(a) shows the experimental results about the variation of γ in the relationship of the applied magnetic field when the width ratios are 0.217, 0.362, 0.464. It is found that γ increases linearly as the magnetic field increases. Figure 6(b) plots the slope of the linear curve to manifest the sensitivity when the width ratios are 0.217, 0.275, 0.319, 0.362, 0.464. The sensitivity reaches the maximum value of approximate 3.31 %/T when the width ratio locates near 0.35 ± 0.02. The trend of the sensitivity change is consistent with the theoretical curve based on the calculation of Eq. (5). The deviation of the experimental results from the theoretical ones is caused mainly by the measurement error of the width of slit and petal-like patterns. According to the relationship of $\frac{\gamma}{B} = \frac{\gamma}{\theta} Vd$, the Verdet constant of the vortex fiber can be estimated to be 0.547 rad/(T·m), which is slightly larger than that of SMF [21]. Such higher Verdet constant is believed to be originated from the high refractive index in the ring core. Moreover, the existing micro-fiber devices can replace the lens, the polarizer, the slit, and highly integrate with PD. Therefore, this developed scheme can realize an all-fiber OAM mode excitation and demodulation system.

IV. Conclusion

In this letter, we have theoretically and experimentally investigated a novel fiber-optic magnetic field sensor by utilizing the vortex fiber that supports OAM $L = \pm 1$ modes opposite circular polarizations, respectively. Based on the circular birefringence property of light beams propagating in vortex fiber when a longitudinal magnetic field is applied, we produced a magnetic-fileld-induced rotation of the interference pattern of superposition of OAM light. Through light intensity after slit change detected by optical power meter, the magnetic field can be obtained conveniently and real-time. A magnetic field sensitivity of 3.31%/T at the width ratio of slit to petal-like patterns of 0.35 ± 0.02 has been demonstrated. This study extends the field of magnetic field sensing by introducing the superposition of OAM modes, and shows OAM fiber modes potential applications in magnetic field sensing and electrical current sensing.

Acknowledgment

The authors thank P. Kristensen from OFS-FITEL for manufacturing the fiber used in our experiments.

References

[1] H. Huang *et al.*, "100 Tbit/s free-space data link enabled by three-dimensional multiplexing of orbital angular momentum, polarization, and wavelength," *Opt. Lett.*, vol. 39, no. 2, pp. 197–200, 2014.
[2] J. Wang *et al.*, "Terabit free-space data transmission employing orbital angular momentum multiplexing," *Nature Photon.*, vol. 6, no. 7, pp. 488–496, 2012.
[3] N. Bozinovic *et al.*, "Terabit-scale orbital angular momentum mode division multiplexing in fibers," *Science*, vol. 340, no. 6140, pp. 1545–1548, Jun. 2013.
[4] A. Wang, L. Zhu, S. Chen, C. Du, Q. Mo, and J. Wang, "Characterization of LDPC-coded orbital angular momentum modes transmission and multiplexing over a 50-km fiber," *Opt. Express*, vol. 24, no. 11, pp. 11716–11726, 2016.
[5] M. Dienerowitz, M. Mazilu, P. J. Reece, T. F. Krauss, and K. Dholakia, "Optical vortex trap for resonant confinement of metal nanoparticles," *Opt. Express*, vol. 16, no. 7, pp. 4991–4999, 2008.
[6] M. Habaza, B. Gilboa, Y. Roichman, and N. T. Shaked, "Tomographic phase microscopy with 180Â° rotation of live cells in suspension by holographic optical tweezers," *Opt. Lett.*, vol. 40, no. 8, pp. 1881–1884, 2015.
[7] D. S. Ding *et al.*, "Quantum storage of orbital angular momentum entanglement in an atomic ensemble," *Phys. Rev. Lett.*, vol. 114, no. 5, Feb. 2015, Art. no. 050502.
[8] R. Fickler, R. Lapkiewicz, M. Huber, M. P. Lavery, M. J. Padgett, and A. Zeilinger, "Interface between path and orbital angular momentum entanglement for high-dimensional photonic quantum information," *Nature Commun.*, vol. 5, p. 4502, Jul. 2014.
[9] M. P. Lavery, F. C. Speirits, S. M. Barnett, and M. J. Padgett, "Detection of a spinning object using lightâĽ™s orbital angular momentum," *Science*, vol. 341, no. 6145, pp. 537–540, Aug. 2013.
[10] R. Lv, L. Qiu, H. Hu, L. Meng, and Y. Zhang, "The phase interrogation method for optical fiber sensor by analyzing the fork interference pattern," *Appl. Phys. B*, vol. 124, no. 2, pp. 124–132, 2018.
[11] L.-Q. Qiu, H.-F. Hu, Y. Zhao, J. Li, and Q. Wang, "Fiber optic temperature sensor using the orbital angular momentum and Gaussian beams," *Instrum. Sci. Technol.*, vol. 45, no. 2, pp. 123–136, Jul. 2016.
[12] S. Shi, D.-S. Ding, Z.-Y. Zhou, Y. Li, W. Zhang, and B.-S. Shi, "Magnetic-field-induced rotation of light with orbital angular momentum," *Appl. Phy. Lett.*, vol. 106, no. 26, Jun. 2015, Art. no. 261110.
[13] S. Yu, F. Pang, H. Liu, X. Li, J. Yang, and T. Wang, "Compositing orbital angular momentum beams in $Bi_4Ge_3O_{12}$ crystal for magnetic field sensing," *Appl. Phys. Lett.*, vol. 111, no. 9, 2017, Art. no. 091107.
[14] P. Gregg, P. Kristensen, and S. Ramachandran, "Conservation of orbital angular momentum in air-core optical fibers," *Optica*, vol. 2, no. 3, pp. 267–270, 2015.
[15] B. Ung, P. Vaity, L. Wang, Y. Messaddeq, L. A. Rusch, and S. LaRochelle, "Few-mode fiber with inverse-parabolic graded-index profile for transmission of OAM-carrying modes," *Opt. Express*, vol. 22, no. 15, pp. 18044–18055, 2014.
[16] T. G. Euser *et al.*, "Birefringence and dispersion of cylindrically polarized modes in nanobore photonic crystal fiber," *J. Opt.Soc. Amer. B, Opt. Phys.*, vol. 28, no. 1, pp. 193–198, 2011.
[17] J. E. Lenz, "A review of magnetic sensors," *Proc. IEEE*, vol. 78, no. 6, pp. 973–989, Jun. 1990.
[18] D. Budker, W. Gawlik, D. F. Kimball, S. M. Rochester, V. V. Yashchuk, and A. Weis, "Resonant nonlinear magneto-optical effects in atoms," *Rev. Modern Phys.*, vol. 74, no. 4, pp. 1153–1201, 2002.
[19] D. M. Palacios, I. D. Maleev, A. S. Marathay, and G. A. Jr. Swartzlander, "Spatial correlation singularity of a vortex field," *Phys. Rev. Lett.*, vol. 92, no. 14, Apr. 2004, Art. no. 143905.
[20] F. Lv, X. Li, Y. Tai, L. Zhang, Z. Nie, and Q. Chen, "High-order topological charges measurement of LG vortex beams with a modified Mach–Zehnder interferometer," *Optik*, vol. 126, no. 23, pp. 4378–4381, Dec. 2015.
[21] J. L. Cruz, M. V. Andres, and M. A. Hernandez, "Faraday effect in standard optical fibers: Dispersion of the effective Verdet constant," *Appl. Opt.*, vol. 35, no. 6, pp. 922–927, 1996.